Hydrol. Earth Syst. Sci. Discuss., 8, 9961–10006, 2011
www.hydrol-earth-syst-sci-discuss.net/8/9961/2011/
doi:10.5194/hessd-8-9961-2011

Hydrology and Earth System Sciences Discussions

A soil moisture and temperature network for SMOS validation in Western Denmark

S. Bircher[1], N. Skou[1], K. H. Jensen[2], J. P. Walker[3], and L. Rasmussen[4]

[1]Technical University of Denmark, DTU Space, Kgs. Lyngby, Denmark
[2]University of Copenhagen, Department of Geography and Geology, Copenhagen, Denmark
[3]Monash University, Department of Civil Engineering, Monash University Victoria, Australia
[4]Aarhus University, Department of Earth Sciences, Aarhus, Denmark

Received: 30 October 2011 – Accepted: 31 October 2011 – Published: 14 November 2011

Correspondence to: S. Bircher (subi@space.dtu.dk)

Published by Copernicus Publications on behalf of the European Geosciences Union.

Abstract

The Soil Moisture and Ocean Salinity Mission (SMOS) acquires surface soil moisture data globally, and thus product validation for a range of climate and environmental conditions across continents is a crucial step. For this purpose, a soil moisture and temperature network of Decagon ECH2O 5TE capacitance sensors was established in the Skjern River Catchment, Denmark. The objectives of this article are to describe a method to implement a network suited for SMOS validation, and to present sample data collected by the network to verify the approach. The design phase included (1) selection of a single SMOS pixel (44 × 44 km), which is representative of the land surface conditions of the catchment and with minimal impact from open water (2) arrangement of three network clusters along the precipitation gradient, and (3) distribution of the stations according to respective fractions of classes representing the prevailing environmental conditions. Overall, measured moisture and temperature patterns could be related to the respective land cover and soil conditions. Texture-dependency of the 0–5 cm soil moisture measurements was demonstrated. Regional differences in 0–5 cm soil moisture, temperature and precipitation between the north-east and south-west were found to be small. A first comparison between the 0–5 cm network averages and the SMOS soil moisture (level 2) product is in range with worldwide validation results, showing comparable trends for SMOS retrieved/initial soil moisture and initial temperature (R^2 of 0.49/0.67 and 0.97, respectively). While retrieved/initial soil moisture indicate significant under-/overestimation of the network data (biases of $-0.092/0.057\,m^3\,m^{-3}$), temperature is in good agreement (bias of $-0.2\,^{\circ}C$). Consequently, the network performs according to expectations and proves to be well-suited for its purpose. The discrepancies between network and SMOS soil moisture will be subject of subsequent studies.

HESSD

8, 9961–10006, 2011

1 Introduction

The assessment of water resources is vital under changing climate and land use, especially when coupled with a steadily increasing population (e.g. FAO-AQUASTAT, 2003). Climate and hydrological models constitute important tools for such investigations, but their reliability is constrained due to uncertainty in important input parameters. One of the key variables is soil moisture, as it significantly impacts water and energy exchanges at the land surface-atmosphere interface, and it represents the main source of water for agriculture and natural vegetation. However, soil moisture is highly variable in space and time and across scales, as a result of spatial heterogeneity in soil and land cover properties, topography and climatic drivers (Famiglietti et al., 1998; Mohanty et al., 2000; Western et al., 2002) rendering it very difficult to assess. Thus, observations of soil moisture at appropriate spatial and temporal scales are urgently needed.

The Soil Moisture and Ocean Salinity satellite (SMOS, Kerr et al., 2001) is the first mission dedicated to soil moisture measurements. A multi-angle, fully polarimetric passive L-band microwave radiometer (1.4 GHz) on board the satellite offers unprecedented possibilities for retrieving surface soil moisture data (~0–5 cm depth) of global coverage every three days at a spatial resolution of ~44 km. However, SMOS data quality is potentially affected by Radio Frequency Interferences (RFI), unresolved image reconstruction issues, errors in both the retrieval algorithm and related input. Thus, it is important that the SMOS algorithm and its associated products be validated by independent in situ measurements across a range of climatic regions.

Generally, such comparisons are complicated by scale-mismatch between the large satellite footprints and the point measurements on the ground (Cosh et al., 2004), entailing the necessity of a high number of distributed observations of the latter to accurately represent the satellite scale. Continuous soil moisture networks have recently evolved across all continents and constitute a core activity in the validation of SMOS data: e.g. USA (Bosch et al., 2006; Schaefer et al., 2007; Jackson et al., 2010); Canada

HESSD
8, 9961–10006, 2011

(Champagne et al., 2010); Australia (Walker et al., 2001; Merlin et al., 2008); Africa (de Rosnay et al., 2009); Europe – Spain (Martinez-Fernandez and Ceballos, 2003), France (Calvet et al., 2007), Germany (Krauss et al., 2010; Bogena et al., 2010). Many of them can be found in the International Soil Moisture Network Database (Dorigo et al., 2011). These networks often face constraints with respect to their density or spatial extent (Cosh et al., 2004). Various upscaling techniques have evolved to derive spatial patterns at large scales, e.g. interpolation (Bardossy and Lehmann, 1998), time/rank stability (Vachaud et al., 1985), statistical transformation (Reichle and Koster, 2004; De Lannoy et al., 2007), and land surface modeling (Crow et al., 2005). However, these methods are sometimes themselves vulnerable to coarse spacing or limited extent of in situ data, often requiring costly long-term pre-studies. Methods to a priori design networks in a spatially representative manner would be beneficial. Friesen et al. (2008) presented an approach of area-weighted sampling by means of landscape units (hydrotopes) with internally more consistent hydrologic behavior, whereby variance and bias in the large-scale in situ soil moisture average can be reduced. The method was successfully applied in two short-term campaigns in West Africa. However, it is both region-dependent and quite complex.

Several studies have focused on the number of samples required to estimate the satellite footprint-scale mean. It was noted that soil moisture variability increases with the spatial extent of a footprint, implying an increase in the necessary number of measurements (Western and Bloeschl, 1999; Famiglietti et al., 1999, 2008). Brocca et al. (2007) found that a minimum of 15 to 35 point samples were required for terrain of negligible to significant topography and an extent of around 5000–10000 m^2. Famiglietti et al. (2008) found a maximum of 30 samples to be required at the 50 km scale assuming independent and spatially uncorrelated data.

A SMOS validation site has been established in the Skjern River Catchment in Western Denmark (Bircher et al., 2011). In the framework of the Hydrological Observatory (HOBE, www.hobe.dk, Jensen and Illangasekare, 2011), a soil moisture and temperature network with 30 stations was installed in fall 2009 within one SMOS pixel

HESSD
8, 9961–10006, 2011

(44 × 44 km) covering large parts of the catchment. In this context, the objectives of this article are (1) to describe a method for the design and implementation of a soil moisture network suited for SMOS validation, and (2) to present the network data set and some analysis including a first comparison with SMOS data to verify the feasibility of our approach, as well as the reliability of the collected data.

The design is split into the selection of (1) an appropriate SMOS pixel, (2) three network clusters within the pixel, and (3) suitable network locations within the clusters. In step 3, a method similar to Friesen et al. (2008) is applied with distribution of the individual stations according to the respective fractions of the prevailing environmental conditions. Friesen et al. (2008) defined the main landscape units a priori, which introduces a risk to exclude important features from the start. In our much simpler method all environmental information is going into the analysis unchanged, whereupon the most important landscape units of the region are detected. Following this approach, it is anticipated that a priori the likelihood of obtaining a representative large-scale in situ soil moisture average for comparison with SMOS data is strongly enhanced.

2 Study area

The Skjern River Catchment is situated in Western Denmark and covers an area of approximately 2500 km^2 (Fig. 1). The climate in the region is temperate-maritime with winter and summer mean temperatures of around 2 and 16 °C, respectively, and an approximate annual precipitation between 800 to 900 mm. The eastern margin of the catchment is situated at the rim of the ice sheet during the latest glacial advance with mainly loamy soils on undulating calcareous tills. The remaining part comprises the primal fluvioglacial outwash plain consisting of low-relief sandy soils and sediments, while poorly drained basins have been filled with organic material (Greve et al., 2007).

The predominant naturally occurring soil type is podsol with a bleached quartz-rich eluviation zone (topsoil) and an illuvation zone (subsoil) usually composed of a hardpan with a black humus-rich band and a subjacent orange-brown layer of sesquioxides

HESSD
8, 9961–10006, 2011

with often distinct mottling (Scheffer and Schachtschabel, 2002). While water drains quickly through the sandy topsoil, this very firm hardpan is almost water tight causing ponding of water at its surface. When fertilized, limed and irrigated high-yield cultivation is possible; this is the case in the major part of the Skjern River Catchment. Intermixed are patches of natural vegetation, i.e. grassland, heath and spruce plantations with pronounced raw humus layers (typically found on podsols). The area is sparsely populated with scattered farms and villages.

Within the catchment four study sites were chosen for the HOBE project (Jensen and Illangasekare, 2011, Fig. 1) to assess a wealth of hydrological parameters. The catchment is well-covered with climate and weather stations operated by the Danish Meteorological Institute (DMI). The 24-h precipitation sums presented in this article are extracted from the DMI 10 × 10 km precipitation grid nodes (Scharling, 1999) contained within the SMOS pixel (Fig. 1). For each day the shelter correction factor of the corresponding month (category B) is applied to the data (Vejen et al., 2000).

3 Data

3.1 Network data

A total of 30 Decagon ECH2O data loggers (Decagon Devices, 2002) were installed, each holding three ECH2O 5TE capacitance sensors measuring soil moisture, temperature, and electrical conductivity (Decagon Devices, 2008) [1]. The 5TE sensors were considered to be a cost-effective solution for large network applications. They are well-suited for measurements in the near-surface layer and they provide integrated measurements over approximately 5–6 cm when installed horizontally (0.3 l measurement volume). Accuracies in mineral soils are ±0.03 and ±1 °C for water content and temperature, respectively. Using the empirical calibration equation of Topp et al. (1980)

[1] Mention of manufacturers is for the convenience of the reader only and implies no endorsement on the part of the authors

HESSD
8, 9961–10006, 2011

volumetric water content is derived from dielectric permittivity, which in turn results from a 5 point dielectric calibration.

The TE sensors (predecessors of 5TE) were excessively tested in soils ranging from 3–100 % sand/0–53 % clay and salt-water solutions of electrical conductivities from 1 to 12 dS m^{-1} by Kizito et al. (2008). They found little probe to probe variability and sufficiently small sensitivity to temperature and electrical conductivity so that one single calibration curve was applicable for all studied conditions. Similarly, for the 5TE sensor type Vasquez and Thomsen (2010) found the Topp equation to be accurate within ±0.02 in the 0–0.5 m depth range at the HOBE agriculture site Voulund (where one network station was placed).

Famiglietti et al. (2008) pointed out, that though site-specific calibration is ideal it is impractical for studies with large sensor numbers distributed over a considerable spatial extent. In their 50 km-scale survey they applied a generalized calibration method with an accuracy of ±0.03 to the entire set of probes, and likewise, this was done by Brocca et al. (2010).

Given the above findings, the Decagon 5TE calibration equation (Topp et al., 1980) has been applied to the network. The given accuracy has been confirmed by some independent testing (addressed in Sects. 4.3 and 5.1).

3.2 SMOS data

The SMOS measurement and soil moisture retrieval concept is complex and will be described to the extent required for understanding the presented work. For further information reference is made to Kerr et al. (2001, 2011).

The radiation collected by the SMOS radiometer is emitted from the area illuminated by the antenna directional gain pattern (working area, ~123 × 123 km). Measurements are made at horizontal and vertical polarizations (H and V) and incidence angles ranging from around 0 to 60° as the satellite passes over the terrain. The working area is characterized by a weighting function resulting in a −3 dB footprint of approximately 44 × 44 km (SMOS pixel).

HESSD
8, 9961–10006, 2011

To derive the level 2 (L2) soil moisture product, brightness temperatures T_B as acquired by SMOS (proportional to the measured radiation) are modeled for both polarizations at each incidence angle by means of the L-band Microwave Emission of the Biosphere (L-MEB) forward model (Wigneron et al., 2007). An initial soil moisture guess and auxiliary parameters (e.g. soil properties, land cover information, leaf area index, topography, temperature and other climate parameters) are required as input. The soil moisture and temperature initial guesses presented in Sect. 5.3.3 both originate from the European Centre for Medium-range Weather Forecasting (ECMWF) product spatially and temporally aggregated over the working area (both contained in the L2 product). Modeled and measured T_Bs are compared, and by minimizing a cost function, soil moisture is iteratively retrieved for each node of a fixed earth surface grid (Discrete Global Grid DGG) with uniform spacing (~15 km). Figure 1 illustrates the locations of the DGG nodes in the Skjern River Catchment, including the working area and corresponding SMOS pixel around one grid node.

L-MEB is based on the relationship between T_B, physical temperature and the land surface emissivity/reflectivity, which in turn is related to the soil's dielectric constant after segregating atmosphere, vegetation and surface roughness contributions using the multi-angular and dual-polarized information. Taking advantage of the large contrast between the dielectric properties of water and solid soil particles at L-band, soil moisture is linked to the dielectric constant via the Dobson dielectric mixing model (Dobson et al., 1985; Peplinski et al., 1995).

L-MEB is built for uniform scenes with certain model characteristics and calibration parameters. However, the above-mentioned auxiliary input parameters are mostly heterogeneous at significantly smaller spatial scales than SMOS pixels. To account for this, the retrieval algorithm aggregates the estimated contributions from several elementary land cover classes derived from ECOCLIMAP (Masson et al., 2003). This data set is previously grouped into eight generic classes (bare soil and low vegetation covers, forests, open water, barren rocks, frozen soils, snow covered areas, ice, and urban areas) and interpolated on a 4 × 4 km reference grid (Discrete Flexible Fine Grid,

HESSD
8, 9961–10006, 2011

DFFG) centered on each DGG node. Within the working area radiometric fractions of each generic land cover class are estimated by means of the antenna weighting function. For the class with the highest radiometric fraction soil moisture is retrieved using the respective elementary model as well as auxiliary input (provided at the DFFG scale), while the other classes contribute with fixed default values.

4 Methodology

4.1 Network design

4.1.1 Selection of SMOS pixel

Two criteria were taken into account when selecting the SMOS pixel to be validated: (1) the spatial overlap between the SMOS pixel and the Skjern River Catchment including the HOBE study sites should be maximized, and (2) the open water fraction within the working area affiliated with the SMOS pixel should be minimized. The latter is of importance as water bodies exhibit very different brightness temperatures than those observed over land, which can significantly impact the soil moisture retrieval result. Eligible SMOS nodes are shown in Fig. 1. Corresponding radiometric open water fractions contained in the respective working areas of DGG nodes 2 001 515, 2 001 516, 2 001 517, 2 002 028, 2 002 029 and 2 002 030 are 1.85, 0.51, 0.29, 0.25, 0.24 and 0.56 %. While all these amounts are very small, the SMOS pixel around node 2 002 029 provides the best coverage of the catchment including the HOBE study sites and was thus chosen for validation.

4.1.2 Selection of network clusters

To minimize maintenance costs the network was designed by dividing the 30 monitoring stations into three clusters with diameters of up to ~10 km (Fig. 2). One cluster was centered on the SMOS grid node as this represents the area from which the highest

HESSD
8, 9961–10006, 2011

radiation fractions originate. A second cluster was allocated to the north-east of the SMOS pixel, around the HOBE agriculture site Voulund with one network station at the study site to render the data connectable to other geophysical measurements. For the same reason one network station was assigned to the HOBE forest site Gludsted, situated some kilometers east of this cluster. The third cluster was placed in the south-west to account for the small spatial gradient observed in the mean annual precipitation for the period 1990 to 2005 (10×10 km grid, Scharling, 1999) from south-west ($\sim$900 mm yr^{-1}) to north-east ($\sim$800 mm yr^{-1}).

4.1.3 Selection of theoretical station locations

For positioning the station locations within these cluster areas, a GIS analysis was performed, thus determining the most representative combinations of environmental conditions (topography, land cover and soil type) within the SMOS pixel. Elevations span from 0 m at the western coastline to around 180 m above sea level in the eastern part of the Skjern River Catchment with 99.8 and 98.5 % of the derived slopes $<5^{\circ}$ for the SMOS pixel and working area of DGG 2 002 029, respectively (90 m digital elevation model of the Shuttle Radar Topographic Mission, Jarvis et al., 2008). No SMOS topography flags are set for node 2 002 029. Consequently, topographical effects were neglected in the successive analysis.

Table 1 summarizes soil types with respective grain size distribution and organic matter content of the 0–20 cm topsoil layer (250 m Danish topsoil grid, Greve et al., 2007). Accordingly, Table 2 shows the subsoil composition below 30 cm depth (clay versus sand) with corresponding clay contents based on a map from (Bornebusch and Milthers, 1935; Smed, 1979; Schou, 1949; DGU, 1945). In both tables respective soil type fractions contained in the SMOS pixel and working area around node 2 002 029 are given. While the pixel comprises almost 80 % coarse sand in the topsoil and 89 % sand in the subsoil, these percentages are lowered to 46 % and 70 % for the entire working area due to a fractional shift towards more loamy soils concurring with the position of the latest glacial ice margin.

HESSD
8, 9961–10006, 2011

Table 3 illustrates land cover fractions (CORINE Land Cover 2000 100 m grid, level 2, EEA, 2005; Bossard et al., 2000) within the SMOS pixel and working area around node 2 002 029, respectively. They are comparable for the two spatial scales with agriculture taking the major parts, followed by forest (mainly coniferous) and shrub/grassland (heath). In agreement with the corresponding SMOS radiometric fractions, water bodies only exhibit marginal parts. Land cover exerts strong influence on the SMOS soil moisture algorithm through both choice of the retrieval model and high non-linearity of vegetation parameters. Thus, it is of importance that the area for which the network delivers soil moisture data is representative for the entire working area in terms of land cover, while this is less relevant in case of soil types.

To find the most representative combinations of topsoil, subsoil, and land cover types within the SMOS pixel, the individual data sets were re-sampled and snapped to the land cover 100 m-grid (Fig. 3a–c). Using the nearest neighbor re-sampling technique merely changed the cell size while all categorical information was conserved. The land cover, top- and subsoil data sets were reclassified to values of 100 s, 10 s and 1 digits ("reclass values" in Tables 1–3), and summed up to one grid containing all possible combinations of the original layers (referred to "composite class map" hereafter, Fig. 3d). Figure 4 displays the composite class fractions revealing five classes (212, 232, 412, 512 and 612) with individual shares of >5 %. Together they constitute approximately 75 % of the SMOS pixel and all have a tendency towards very sandy soils. Including the most frequent classes with humus in the topsoil (292) and clay in the subsoil (211), ~82 % of the prevailing environmental conditions in the validation area are incorporated, which is regarded as a good overall representation. As CORINE land cover class 400 (heterogeneous agriculture) contains all prevailing land cover types (arable land intermixed with forest and shrub/grassland, Bossard et al., 2000), the composite class 412 was repartitioned equally to the classes 212 and 612 (same soil type, Table 4). The 30 network stations were then distributed among these six classes according to their respective fractions.

HESSD
8, 9961–10006, 2011

Plant structure has an influence on vegetation parameters in the SMOS soil moisture algorithm. Thus, the predominant crop types were estimated based on the field plan 2005 (FVM, 2005) as well as areal cultivation statistics 2006–2008 (Danmarks Statistik and Service, 2009, Table 5) for Central Western Denmark. The 22 agricultural network stations were allocated to fields with the three most frequent crops barley, grass and winter wheat, and additionally to maize and potatoes (differing plant structure) according to respective fractions.

4.2 Network implementation

4.2.1 Field inspection/final decision on station locations

Provisionally, the stations were distributed among the three network clusters using the composite class map (Fig. 3d). Final decisions on the locations were taken after field inspection. Due to an extensive road network, access did not constrain the choice.

For forest and heath (composite classes 512 and 612), no reallocation of the preselected points was necessary, as theoretically estimated land cover and soil types were in good agreement with actual conditions. Three stations were placed under scotch heather, one under natural grass, and four under spruce plantations characterized by pronounced row structure, scarce understory and moss carpets. All these locations exhibit distinct organic surface layers.

The estimated occurrence of agricultural areas and crop types was also encountered in reality, and in case of the composite class 212 the expected very sandy top- and subsoils were clearly perceived at the preselected locations. However, the distinction between classes 212 and 292 (sand and humus in the topsoil, respectively) was almost impossible, as the upper soil layer exhibited a very dark color at all investigated locations, due to intermixed organic matter as a result of agricultural practices. Likewise, for locations where classes with higher clay fractions were indicated on the composite class map (i.e. class 211 with clay in the subsoil or class 232 with loamy sand in the top soil) we could solely notice that soils clearly exhibited greater clay contents than

HESSD
8, 9961–10006, 2011

the sandy classes. In situ discrimination between class 211 and 232 turned out to be difficult. Furthermore, at locations where an increased clay fraction was noticed, it persisted usually throughout the entire depth profile. As classes 211, 232 and 292 only account for a small fraction of the entire SMOS pixel (~13 %), these inaccuracies were accepted when placing the corresponding stations. We resigned the labor-intensive determination of texture and organic amounts for the localization of spots with the exact soil properties inherent in the respective composite classes. Two of the four more clayey stations were placed outside of the third cluster in the south-east to account for the region where the main fraction of more clayey soil conditions within the SMOS pixel occurs as a result of the geomorphological evolution in the area (see Sect. 2).

The estimated number of stations per crop type could be maintained, even though some adjustments had to be made between the composite classes (Table 5). This was accepted since crop rotations change throughout the years. An overview of the final network locations is given in Fig. 2 and Table 6.

4.2.2 Installation

Sensor installation took place in fall 2009. At each station, three 5TE sensors were placed at respective depths of 2.5, 22.5 and 52.5 cm (corresponding to measurement intervals of ~0–5, 20–25 and 50–55 cm) from the soil surface after removal of the litter/organic layer (Fig. 5). The sensors were horizontally inserted with the blade in the vertical position to avoid ponding.

While for SMOS validation the 0–5 cm data is of most importance, the profile measurements suit the needs of hydrological modeling activities in the HOBE project, possibly in combination with assimilated SMOS data. With respect to heath and forest stations, one 5TE sensor was additionally installed in the organic layer in summer 2010. This is crucial as the signal measured by SMOS over these areas most probably originates exclusively from this moist layer (Bircher et al., 2010).

HESSD
8, 9961–10006, 2011

Sensor readings are logged in 30 min intervals. Stations placed in crops have to be temporarily removed during cultivation practices (seed/plantation and harvest) – twice for summer crops (spring and fall) and once for winter crops (late summer).

Soil samples were taken at each sensor depth during installation. Sand (2000–20 µm), silt (20–2 µm) and clay (<2 µm) fractions (International Society of Soil Science, ISSS, 1929) of the 0–5 cm depth were determined for all network locations using sedimentation and sieve analysis, and soil bulk density was calculated (Table 6). Additionally, soil samples were collected from 0–5 cm depth on agricultural land, forest and heath (composite classes 212, 512 and 612, resp.) during an airborne campaign (Bircher et al., 2011). These samples were used for calibration checks over the entire wetness range in the laboratory.

4.3 Network data analysis

To check the feasibility of our approach as well as the reliability of the network data, several analyses were conducted:

The sensor output – sample water content couples from the lab calibration were compared to the Decagon 5TE default calibration curve (Topp et al., 1980). By means of the texture data the actual soil type distribution among the network stations was compared with the one based on the composite class map. Per station the measured soil moisture and temperature data of all depths for the year 2010 was checked for the expected behavior as a function of land cover and soil types.

Further network data analyses focused on the 0–5 cm depth only:

1. The soil moisture data of five selected agricultural stations (2.09, 3.08, 3.01, 1.09, and 3.05, Fig. 2/Table 6) with vegetation types of comparable plant structure but decreasing clay (21–2 %)/increasing sand (51–95 %) fractions was compared with the 30 station network average in order to study the influence of texture for the time period January–August 2010 (to assure continuous data coverage).

HESSD
8, 9961–10006, 2011

2. To study regional variability and potential influence of the long-term precipitation gradient, soil moisture and temperature of three selected stations of similar texture and land cover in the north-east (1.02, 1.06, 1.09) and south-west part (3.02, 3.04, 3.07) of the SMOS pixel as well as precipitation data of the two closest 10 km grid nodes, respectively, were averaged and compared over the year 2010.

3. Soil moisture and temperature averaged over all 30 network stations were compared with SMOS L2 soil moisture (initial guess and retrieved) and temperature (initial guess) data for the year 2010. Furthermore, to avoid deviations that may arise from the applied petrophysical relationship (Topp et al., 1980), this comparison was also conducted at the dielectric constant level. The 5TE sensor output was transformed to the real part of the dielectric constant by both the Decagon conversion (output/50) as well as an empirical relationship (real dielectr. = 0.0234*output-1.2917, Rosenbaum et al., 2010), and averaged over all 30 network stations. With respect to SMOS, the real part of the dielectric constant from the L2 product (retrieved with a non cardioid model, Bengoa et al., 2010) computed from the retrieved soil moisture data by means of the Dobson dielectric mixing model was used.

5 Results and discussion

5.1 Calibration and soil texture checks (0–5 cm)

Figure 6 shows the 5TE sensor output compared to the volumetric moisture content derived from 0–5 cm soil samples collected on agricultural land, forest and heath (composite classes 212, 512 and 612, resp.) as well as the Decagon 5TE default calibration curve. Corresponding Root Mean Square Error (RMSE) values are 0.030, 0.026 and 0.022. Thus, for all three classes RMSEs are within the declared sensor accuracy (0.030).

HESSD
8, 9961–10006, 2011

In Fig. 7 the 0–5 cm depth texture data (sand-% vs. clay-%) for the network are shown and compared to the composite classes used in the Danish soil grid (Greve et al., 2007). As the organic content was not measured it is not possible to classify the two stations representing class 292. For the remaining 28 stations it can be seen that: (1) all forest and heath stations (classes 512 and 612) are correctly allocated to the soil type sand, while two of the agriculture class 212 (stations 2.04 and 2.08) exhibit slightly higher clay fractions than expected; (2) the agriculture class 211 is expected only to show more clay conditions in the subsoil, but in fact slightly and significantly higher clay fractions in the topsoil are found for stations 3.01 and 3.08, respectively; (3) with respect to agricultural class 232 station 3.09 is correctly classified whereas station 2.09 shows significantly higher clay fractions than expected. Overall, five out of 28 stations are misclassified. However, overall the predetermined number of stations per soil type (Table 4) is more or less maintained in the final network setup.

5.2 Profile soil moisture and temperature (all depths)

Figure 8 shows soil and temperature data of all depths acquired during the year 2010 for five selected stations representing the majority of encountered patterns throughout the entire network data set: 2.11 (heath, class 612), 1.04 (forest, class 512), 1.02 (agriculture, class 212, HOBE site Voulund), 2.05 (agriculture, class 212), and 2.09 (agriculture, class 232). Additionally, in case of the heath and forest stations (2.11 and 1.04) data from the sensors installed in the organic layers are depicted. It should be noted that for the organic material, site-specific calibration will be a crucial issue. Thus, at the point of writing this paper these measurements should only be considered in a relative term.

Typically, for all network locations in agricultural fields and with coarse sand in the topsoil, a homogeneous mixture of loose sand and organic material is found in the plow layer with a pronounced hardpan just below (~30–45 cm depth), and with sand appearing at around ~35–50 cm depth. Litter is absent or scarce, never covering the

HESSD
8, 9961–10006, 2011

surface as a whole. In most cases the 0–5 cm and 20–25 cm sensors were installed in the plow layer. As water infiltrates quickly through the sandy material and the water content in the surface layer is reduced by evapotranspiration, the 0–5 cm sensors generally show drier conditions than the 20–25 cm sensors located just above the hardpan, which restricts the further downward movement of water. Moreover, the 50–55 cm sensors measure high water contents if located close to the upper hardpan boundary (station 1.02) and show much drier conditions when installed within or below the hardpan (station 2.05).

In contrast, a pronounced litter layer of moss/organic material exists (~5–20 cm) for the sandy soils under natural vegetation. Due to absence of plowing, the topsoil down to the hard pan is leached and quartz-rich as expected for a typical podsol, and the hardpan starts at around 20–25 cm depth. While all four forest stations show similar soil moisture patterns throughout time, the conditions at the four heath stations are very variable. Station 2.11, for instance, is situated in a very wet area where standing water was observable around the station during installation. The 0–5 cm sensor at this station shows high moisture values as it is nourished by the very moist moss/organic layer on top. At the time of installation the 50–55 cm sensor was mounted below the water table. However, when the water table later during the season was lower the effect of the dry sand below the hardpan became evident in the data from the 50–55 cm sensor. In comparison, the sensors in the moss/organic layer as well as the 0–5 cm mineral layer of the forest station 1.04 show much drier conditions. This can be attributed to their placement on a small hill. The 20–25 cm sensors ob both stations 2.11 and 1.4 were installed at the upper hardpan boundary and show similar behavior. Generally, the pattern of the forest stations is more related to the one met at agriculture sites where the 50–55 cm sensor is located in the dry sand below the hardpan (station 2.05).

At station 2.09 the sensors were installed in clayey material with much higher water holding capacity throughout the entire depth profile, and with a firm hardpan at 20–25 cm depth. During installation the water table was at 20 cm depth. Later during the

HESSD
8, 9961–10006, 2011

summer the soil at the 20–25 cm sensor location became drier while the 50–55 cm sensor remained below the water table.

The different values for porosity of sandy and clayey soils are well-reflected in the measurements of the 50–55 cm sensors situated below the water table with saturated moisture contents of ~0.4 and 0.5 in case of the sandy station 2.11 and the clayey station 2.9, respectively. Even higher values are found in the organic material. Furthermore, the effect of texture is also reflected in the seasonal variation of soil moisture for the different soil types. Sandy soils have a smaller water holding capacity compared to clayey and organic materials and as a result the seasonal variation is relatively small. Apart from the drop of moisture content in the organic and 0–5 cm mineral layers during freezing in the winter months this behavior is evident for the two sandy agricultural stations (1.02 and 2.05) as well as for the forest station (1.04). In contrast, the clayey agricultural station (2.09) and the heath station (2.11) show a much higher seasonal variability. Irrigation has obviously a distinct imprint as seen for the agricultural stations 1.02 and 2.05, and in case of the forest site, tree interception must exert a balancing effect.

At all sites the temperature profiles show the expected diurnal and seasonal patterns, as well as a slight time lag and amplitude decrease with increasing depth. Furthermore, the presence of vegetation and moss/organic layers (heath and forest stations) insulating the mineral soil becomes apparent. The isolation effect is reflected in both the diurnal and seasonal temperature amplitudes and is most pronounced for the forest station.

All in all the observed moisture and temperature patterns are clearly related to land cover and soil conditions. Soil moisture seems to be mostly affected by soil characteristics while soil temperature is mostly dependent on land cover.

HESSD
8, 9961–10006, 2011

5.3 Surface soil moisture and temperature (0–5 cm)

5.3.1 Texture comparison

Figure 9 illustrates the 0–5 cm soil moisture measurements of the agricultural stations 2.09, 3.08, 3.01, 1.09 and 3.05 with similar vegetation and decreasing clay/increasing sand fractions (Table 6), respectively, in comparison with the 0–5 cm average over all 30 stations between January and August 2010. The mean of daily precipitation of the 10 km grid nodes contained within the SMOS pixel (Fig. 1) is also plotted.

Over the major part of the chosen time span, increasing clay content complies with higher moisture content, resulting in significant overrepresentation with respect to the overall network average, and vice versa in the case of high sand contents. Thus, the influence of soil texture is clearly demonstrated and also reflected in the biases (average residuals from expected value) ranging from 0.146 for the clay station 2.09 to −0.057 for station 3.05 with highest sand fractions. The larger absolute bias (relative to other stations) of the clay station is reasonable, as the 30 station average contains a much larger fraction of sandy sites. The moisture pattern also follows the precipitation trend well, and in March, snow melt is observable throughout all stations.

5.3.2 Regional comparison

Figure 10 shows average and standard deviation (shaded region) of the 0–5 cm soil moisture and temperature of three selected stations of similar texture and land cover in the north-east (1.02, 1.06, 1.09) and south-west part (3.02, 3.04, 3.07) of the SMOS pixel, as well as 24 h precipitation accumulations of the two closest 10 km grid nodes, respectively, for the year 2010.

Regional differences are most pronounced for soil moisture and least for temperature. However, in any case they are small with low RMSE/biases (0.034/0.010, 0.86/0.11 °C and 3.72/−0.39 mm for soil moisture, temperature and precipitation, respectively), with considerable correlations reflected in corresponding R^2 values of 0.57,

HESSD
8, 9961–10006, 2011

0.99 and 0.86. Moreover, with temporal mean standard deviations of 0.024 and 0.041 (soil moisture) and 0.37 and 0.5 °C (temperature) for the north-eastern and south-western stations, respectively, the variability between the two areas is in the same order as within them.

5.3.3 SMOS L2 comparison

Figure 11 displays 0–5 cm average network and SMOS soil moisture and temperature data (L2 product) for the year 2010, as well as the corresponding mean of daily precipitation of the DMI 10 km grid nodes contained within the SMOS pixel (Fig. 1).

Also network soil moisture spatial variability (standard deviation, blue shaded region) and in situ sensor accuracy are shown (grey shaded region). For SMOS retrieved values and associated radiometric accuracies (shaded region) as well as the initial guess are shown. Mean network soil moisture fluctuates around a temporal average of 0.176 and with a standard deviation of 0.041. The spatial variability between the individual stations is larger with a temporal average of 0.070, which is in the same order as found by Famiglietti et al. (2008) for a site in the United States at the same spatial scale. Network and SMOS soil moisture follow the precipitation dynamics well. Correlations (R^2) between network and SMOS retrieved and initial guess soil moisture, respectively are 0.49 and 0.67. However, remarkable offsets are visible. While the SMOS soil moisture initial guess approximately corresponds to the upper boundary of the network variability error bar, the retrieved data follows more or less its lower boundary, or even below (bias values of 0.057/−0.092 for initial/retrieved SMOS soil moisture compared to the network average, respectively). Furthermore, SMOS soil moisture shows higher amplitude compared to the network data. These findings are consistent with results from various validation sites across continents: Australia (Ruediger et al., 2011), Germany (Dall'Amico et al., 2011), USA (Jackson et al., 2011; Al Bitar et al., 2011; Leroux et al., 2011) report positive biases in the order of 0.05–0.15 and negative biases around 0.02–0.2 for SMOS initial and retrieved soil moisture, respectively. The temporal trends encountered at the individual sites are followed by the retrieved SMOS soil moisture

HESSD
8, 9961–10006, 2011

($R^2 \sim 0.4$–0.62), and tendencies of the latter to overestimate the dynamics (larger amplitudes) have also been noted. Only in Africa constant soil moisture overestimation by SMOS was found (Gruhier et al., 2011).

In case of temperature, the average of the 30 network stations and the SMOS initial guess surface temperature are in good agreement with corresponding RMSE, bias and R^2 values of 1.1 °C, −0.2 °C and 0.97, respectively. Thus, no significant error seems to be introduced from this parameter.

The comparison of the real dielectric constant averaged from the network and for SMOS over the year 2010 reveal RMSE, bias and R^2 values of 3.95/4.30, 2.30/3.33 and 0.49/0.49 for the Decagon/Rosenbaum et al. (2010) sensor output-dielectric constant relations, respectively. Consequently, there is no distinct difference between the two dielectric models with R^2s equal to that for the soil moisture comparison. As the SMOS dielectric constant is computed from retrieved soil moisture by means of the Dobson model, this implies that at both comparison levels the uncertainty is consistent and remains on either the network or the SMOS data side.

Based on the results of the presented network data analyses together with the fact that our findings from the comparison with SMOS data are well in range with worldwide validation results, we consider the network to operate according to expectations and to be well-suited for SMOS validation. The discrepancies between network and retrieved SMOS soil moisture data need to be more closely investigated. Currently, numerous explanations are under discussion: (1) a mismatch between sampling depth of conventional soil moisture sensors (~5–7 cm) and the depth contributing to L-band soil emission (<5 cm, Escorihuela et al., 2010), (2) scale effects due to the large disparity in spatial scale between the SMOS and in situ measurements, (3) inaccuracies in the SMOS retrieval algorithm and related input, (4) inacurracies in the in situ measurements, and (5) RFI contamination. It is likely, that the observed deviations result from a combination of these factors with variable contributions depending on a validation site's environmental conditions as well as the chosen measurement setup. At the Danish validation site, for example, we believe to reduce the probability of scaling effects by

HESSD
8, 9961–10006, 2011

means of the carefully chosen network setup. Meanwhile, we see RFI contamination and inaccuracies in the SMOS retrieval algorithm as probable causes for the bias. Currently, the replacement of the Dobson dielectric mixing model with the one of Mironov (Mironov et al., 2004) is for example under investigation. Bircher et al. (2011) showed that Mironov performed better at the Danish validation site to bring brightness temperatures modeled from in situ soil moisture data in agreement with airborne brightness temperature measurements at the 2 × 2 km scale. Thus, it is also likely that the deviances between SMOS and in situ soil moisture could be lowered by using Mironov in the SMOS retrieval algorithm. With respect to the high amplitudes in the retrieved SMOS data, there is generally consensus that they are likely to be attributed to the mismatch in sampling depth. Generally, the very top layer shows a rapid soil moisture increase immediately following rain events, succeeded by a fast decrease as a result of evaporation and infiltration processes. At deeper depths this response is delayed and somewhat less. The wetter and the more sandy the soils, the more pronounced this effect is. However, at this point, this remains a hypothesis. Further investigations are needed to separate the respective contributions to the deviations between in situ data and SMOS and thus clarify these issues.

6 Conlusions

A soil moisture and temperature network with 30 stations (sensors at 0–5, 20–25 and 50–55 cm depths plus in the organic layer in the case of heath/forest locations) has been established within one SMOS pixel (44 × 44 km) in the Skjern River Catchment, Western Denmark

The design of the network included the following phases: (1) the selection of SMOS pixel 2 002 029 with minimal water fraction and maximal catchment coverage, (2) the arrangement of three network clusters along a long-term precipitation gradient centered at the SMOS node, and (3) the distribution of the stations according to respective fractions of six classes combining 82 % of the prevailing land cover, top- and subsoil

HESSD
8, 9961–10006, 2011

conditions. In case of agriculture, additionally crop type frequency was considered. Using this method, it was possible to obtain a representative large-scale in situ soil moisture average for comparison with SMOS data.

Analysis of the collected network data during the year 2010 showed that soil moisture generally follows the precipitation trend. Furthermore, soil moisture and temperature patterns were relatable to the respective land cover and soil conditions. The high soil moisture variability throughout the stations seems to be a strong function of texture/structure while to a less extent influenced by land cover. At the same time the variability in soil temperature is less pronounced and merely a function of the latter. Regional differences in 0–5 cm soil moisture, temperature and precipitation between the north-east and south-west turned out to be small.

A first comparison between 0–5 cm network averages and the SMOS L2 product showed comparable trends with R^2 of 0.49/ 0.67 and 0.97 for SMOS retrieved/initial soil moisture and initial temperature, respectively. The two former indicate significant under-/overrepresentation of the network data (biases of $-0.092/0.057\,m^3\,m^{-3}$) as well as faster and stronger wetting/dry-downs (larger amplitudes). Correlation with precipitation is traceable in both, network and SMOS soil moisture data. Average network and SMOS soil temperatures are in good agreement with a bias of $-0.2\,^{\circ}C$. Thus, this parameter should not introduce errors in the soil moisture retrieval process.

Based on these findings together with the fact that our SMOS data comparison is well in range with worldwide validation results, we consider the network to operate according to expectations and to be suitable for SMOS validation. Extensive validation activities are currently ongoing at the Danish validation site. It is likely that the discrepancies between network and SMOS soil moisture result from a combination of several factors. The investigation of these potential error sources and their respective contributions is subject of subsequent studies. Furthermore, the influence of the organic layers under natural vegetation is planned to be addressed.

HESSD
8, 9961–10006, 2011

Acknowledgements. The project was funded by the Villum Foundation and the Technical University of Denmark. Special thank goes to Yann Kerr and his team at CESBIO, and Jean-Pierre Wigneron for constructive discussions. We also gratefully appreciate various support of the HOBE project members throughout this work.

References

Al Bitar, A., Leroux, D., Kerr, Y., Merlin, O., Richaume, P., Sahoo, A., and Wood, E. F.: Evaluation of SMOS Soil Moisture products over continental US using the SCAN/SNOTEL network, IEEE T. Geosci. Remote Sens., in review, 2011. 9980

Bardossy, A. and Lehmann, W.: Spatial distribution of soil moisture in a small catchment, Part 1: geostatistical analysis, J. Hydrol., 206, 1–15, 1998. 9964

Bengoa, B., Zapata, M., Cabeza, C., and Rodriguez, M.: SMOS Level 2 processor and Auxiliary Data Products Specifications, Tech. Rep. SO-TN-IDR-GS-0006, V5.3, INDRA, Madrid, available at: http://www.cesbio.ups-tlse.fr/fr/indexsmos.html, 2010. 9975

Bircher, S., Balling, J., and Skou, N.: SMOS validation activities at different scales in the Skjern River Catchment, Western DK, in: ESA Living Planet Symposium, edited by: Lacoste-Francis, H., ESA, ESA communications, Bergen, Norway, 2010. 9973

Bircher, S., Balling, J. E., Skou, N., and Kerr, Y.: Validation of SMOS brightness temperatures during the HOBE airborne campaign, Western Denmark, IEEE T. Geosci. Remote Sens., accepted, doi:10.1109/TGRS.2011.2170177, 2011. 9964, 9974, 9982

Bogena, H., Herbst, M., Huisman, J. A., Rosenbaum, U., Weuthen, A., and Veerecken, H.: Potential of wireless sensor networks for measuring soil water content variability, Vadose Zone J., 9, 1002–1013, 2010. 9964

Bornebusch, C. and Milthers, K.: Jordbundskort over Danmark, 1:500.000, Danmarks Geologiske Undersoegelse, 111:24, 1935. 9970

Bosch, D., Lakshmi, V., Jackson, T., Choi, M., and Jacobs, J.: Large scale measurements of soil moisture for validation of remotely sensed data: Georgia soil moisture experiment of 2003, J. Hydrol., 323, 120–137, 2006. 9963

Bossard, M., Feranec, J., and Otahel, J.: CORINE land cover technical guide – Addendum 2000, Tech. Rep. 40, European Environmental Agency, Copenhagen, available at: http://www.eea.europa.eu/publications/tech40add, 2000. 9971

HESSD

8, 9961–10006, 2011

Brocca, L., Morbidelli, R., Melone, F., and Moramarco, T.: Soil moisture spatial variability in experimental areas of central Italy, J. Hydrol., 333, 356–373, 2007. 9964
Brocca, L., Melone, F., Moramarco, T., and Morbidelli, R.: Spatial-temporal variability of soil moisture and its estimation across scales, Water Resour. Res., 46, W02516, doi:10.1029/2009WR008016, 2010. 9967
Calvet, J.-C., Fritz, N., Froissard, F., Suquia, D., Petitpa, A., and Piguet, B.: In situ soil moisture observations for the CAL/VAL of SMOS: the SMOSMANIA network, in: IEEE Int. Geosci. Remote Se. (IGARSS), 1196–1199, Barcelona, Spain, 2007. 9964
Champagne, C., Berg, A., Belanger, J., McNairn, H., and de Jeu, R.: Evaluation of soil moisture derived from passive microwave remote sensing over agricultural sites in Canada using ground-based soil moisture monitoring networks, Int. J. Remote Sens., 31, 3669–3690, 2010. 9964
Cosh, M., Jackson, T., Bindlish, R., and Prueger, J. H.: Watershed scale temporal and spatial stability of soil moisture and its role in validating satellite estimates, Remote Sens. Environ., 92, 427–435, 2004. 9963, 9964
Crow, W. T., Ryu, D., and Famiglietti, J. S.: Upscaling of field-scale soil moisture measurements using distributed land surface modeling, Adv. Water Resour., 28, 1–14, 2005. 9964
Dall'Amico, J. T., Schlenz, F., Loew, A., and Mauser, W.: First results of SMOS soil moisture validation in the Upper Danube Catchment, IEEE T. Geosci. Remote Sens., accepted, 2011. 9980
Danmarks Statistik, A. and Service, H.: Cultivated area by unit, region, crop and time in hectares for the region Midtjylland, available at: www.statistikbanken.dk, verified 10 June 2009, 2009. 9972
De Lannoy, G. J. M., Houser, P. R., Verhoest, N. E. C., Valentijn, V. R. N., and Gish, T. J.: Upscaling of point soil moisture measurements to field averages at the OPE test site, J. Hydrol., 343, 1–11, 2007. 9964
de Rosnay, P., Gruhier, C., Timouk, F., Baup, F., Mougin, E., Hiernaux, P., Kergoat, L., and LeDantec, V.: Multi-scale soil moisture measurements at the Gourma meso-scale site in Mali, J. Hydrol., 375, 241–252, 2009. 9964
Decagon Devices, I.: ECH2O data collection system. Operator's manual for models Em50/Em50R., Decagon Devices, Inc., 2365 NE Hopkins Court Pullman WA 99163 USA, version 6 Edn., 2002. 9966
Decagon Devices, I.: ECH2O soil moisture sensor. Operator's manual for model 5TE., Decagon

HESSD
8, 9961–10006, 2011

Devices, Inc., 2365 NE Hopkins Court Pullman WA 99163 USA, version 3 Edn., 2008. 9966
DGU: Geologiske kort over Danmark, 1:100.000, D.G.U, 1945. 9970
Dobson, M., Ulaby, F., Hallikainen, M., and El-Reyes, M.: Microwave dielectric behavior of wet soil – Part II: Dielectric mixing models, IEEE T. Geosci. Remote Sens., 23, 35–46, 1985. 9968
Dorigo, W. A., Wagner, W., Hohensinn, R., Hahn, S., Paulik, C., Drusch, M., Mecklenburg, S., van Oevelen, P., Robock, A., and Jackson, T.: The International Soil Moisture Network: a data hosting facility for global in situ soil moisture measurements, Hydrol. Earth Syst. Sci. Discuss., 8, 1609–1663, doi:10.5194/hessd-8-1609-2011, 2011. 9964
EEA: Corine land cover 2000 (CLC2000) 100 m – version 8/2005, available at: http://dataservice.eea.eu.int/, 2005. 9971
Escorihuela, M., Chanzy, A., Wigneron, J., and Kerr, Y.: Effective soil moisture sampling depth of L-band radiometry: A case study, Remote Sens. Environ., 114, 995–1001, 2010. 9981
Famiglietti, J., Devereaux, J., Laymon, C., Tsegaye, T., Houser, P., Jackson, T., Graham, S., Rodell, M., and van Oevelen, P.: Ground-based investigations of soil moisture variability within remote sensing footprints during the Southern Great Plains 1997 (SGP97) Hydrology Experiment, Water Resour. Res., 35, 1839–1851, 1999. 9964
Famiglietti, J. S., Rudnicki, J. W., and Rodell, M.: Variability in surface moisture content along a hillslope transect: Rattlesnake Hill, Texas, J. Hydrol., 210, 259–281, 1998. 9963
Famiglietti, J. S., Ryu, D., Berg, A. A., Rodell, M., and Jackson, T. J.: Field observations of soil moisture variability across scales, Water Resour. Res., 44, W01423, doi:10.1029/2006WR005804, 2008. 9964, 9967, 9980
FAO-AQUASTAT: Review of world water resources by country, available at: http://www.fao.org/nr/water/aquastat/main/index.stm, 2003. 9963
Friesen, J., Rodgers, C., Oguntunde, P. G., Hendrickx, J. M. H., and van de Giesen, N.: Hydrotope-based protocol to determine average soil moisture over large areas for satellite calibration and validation with results from an observation campaign in the Volta Basin, West Africa, IEEE T. Geosci. Remote Sens., 46, 1995–2004, 2008. 9964, 9965
FVM: Information on crops on field level from the Ministry of Food, Fisheries and Agriculture (FVM) regarding application for single-payments in 2005., accessed via the research-based agricultural registry at The Faculty of Agriculture, Aarhus University., 2005. 9972
Greve, M. H., Greve, M. B., Bøcher, P., Balstrøm, T., Breuning-Madsen, H., and Krogh, L.: Generating a Danish raster-based topsoil property map combining choropleth maps and

HESSD
8, 9961–10006, 2011

point information, Danish Journal of Geography, 107, 1–12, 2007. 9965, 9970, 9976, 10002
Gruhier, C., Pellarin, T., de Rosnay, P., and Kerr, Y.: SMOS soil moisture product evaluation over West-Africa at local and regional scale, Remote Sens. Environ., in review, 2011. 9981
ISSS: Minutes of the First Commission Meetings, in: Proceedings of the International Society of Soil Science, vol. 4, 215–220, International Society of Soil Science (ISSS), Washington, USA, 1929. 9974
Jackson, T. J., Cosh, M. H., Bindlish, R., Starks, P. J., Bosch, D. D., Seyfried, M., Goodrich, D. C., Moran, M. S., and Du, J.: Validation of Advanced Microwave Scanning Radiometer soil moisture products, IEEE T. Geosci. Remote Sens., 48, 4256–4272, 2010. 9963
Jackson, T. J., Bindlish, R., Cosh, M., Zhao, T., Starks, P. J., Bosch, D. D., Seyfried, M., Moran, S. M., Goodrich, D., Kerr, Y., and Leroux, D.: Validation of Soil Moisture and Ocean Salinity (SMOS) soil moisture over watershed networks in the US, IEEE T. Geosci. Remote Se., accepted, 2011. 9980
Jarvis, A., Reuter, H., Nelson, A., and Guevara, E.: Hole-filled seamless SRTM, data V4, available at: http://srtm.csi.cgiar.org, 2008. 9970
Jensen, K. and Illangasekare, T.: HOBE: A Hydrological Observatory, Vadose Zone J., 10, 1–7, 2011. 9964, 9966
Kerr, Y., Waldteufel, P., Wigneron, J.-P., Martinuzzi, J.-M., Font, J., and Berger, M.: Soil moisture retrieval from space: The soil moisture and ocean salinity (SMOS) mission, IEEE T. Geosci. Remote Sens., 39, 1729–1735, doi:10.1109/36.942551, 2001. 9963, 9967
Kerr, Y., Waldteufel, P., Richaume, P., Davenport, P., Ferrazzoli, P., and Wigneron, J.-P.: SMOS level 2 processor Soil Moisture Algorithm theoretical Basis Document (ATBD), Tech. Rep. SO-TN-ARR-L2PP-0037, V3.4, CBSA, UoR, TV and INRA, Toulouse, available at: http://www.cesbio.ups-tlse.fr/fr/indexsmos.html, 2011. 9967
Kizito, F., Campbell, C. S., Campbell, G. S., Cobos, D., Teare, B., Carter, B., and Hopmans, J.: Frequency, electrical conductivity and temperature analysis of a low-cost capacitance soil moisture sensor, J. Hydrol., 352, 367–378, 2008. 9967
Krauss, L., Hauck, C., and Kottmeier, C.: Spatio-temporal soil moisture variability in Southwest Germany observed with a new monitoring network within the COPS domain, Meteorolog. Z., 19, 523–537, 2010. 9964
Leroux, D. J., Kerr, Y. H., Al Bitar, A., Gruhier, C., Bindlish, R., Jackson, T. J., Berthelot, B., and Portet, G.: Comparison between SMOS and other satellite and model forecast products, Remote Sens. Environ., in review, 2011. 9980

HESSD
8, 9961–10006, 2011

Martinez-Fernandez, J. and Ceballos, A.: Temporal stability of soil moisture in a large-field experiment in Spain, Soil Sci. Soc. Am. J., 67, 1647–1656, 2003. 9964
Masson, V., Champeaux, J., Chauvin, F., Meriguet, C., and Lacaze, R.: A global database of land surface parameters at 1 km resolution in meterological and climate models, J. Climate, 16, 1261–1282, 2003. 9968
Merlin, O., Walker, J., Kalma, J., Kim, E., Hacker, J., Panciera, R., Young, R., Summerell, G., Hornbuckle, J., Hafeez, M., and Jackson, T.: The NAFE'06 data set: Towards soil moisture retrieval at intermediate resolution, Adv. Water Resour. Res., 31, 1444–1455, 2008. 9964
Mironov, V., Dobson, M., Kaupp, V., Komarov, S., and Kleshchenko, V.: Generalized refractive mixing dielectric model for moist soils, IEEE T. Geosci. Remote Se., 42, 773–785, 2004. 9982
Mohanty, B. P., Skaggs, T. H., and Famiglietti, J. S.: Analysis and mapping of field-scale soil moisture variability using high-resolution, ground-based data during the Southern Great Plains 1997 (SGP97) Hydrology Experiment, Water Resour. Res., 36, 1023–1031, 2000. 9963
Peplinski, N., Ulaby, F., and Dobson, M.: Dielectric properties of soils in the 0.3-1.3-GHz range, IEEE T. Geosci. Remote Se., 33, 803–807, 1995. 9968
Reichle, R. and Koster, R.: Bias reduction in short records of satellite soil moisture, Geophys. Res. Lett., 31, L19501, doi:10.1029/2004GL.020938, 2004. 9964
Rosenbaum, U., Huisman, J., Weuthen, A., Vereecken, H., and Bogena, H.: Sensor-to-sensor variability of the ECH2O EC-5, TE and 5TE sensors in dielectric liquids, Vadose Zone J., 9, 181–186, 2010. 9975
Ruediger, C., Walker, J. P., Kerr, Y. H., Mialon, A., Merlin, O., and Kim, E. J.: Validation of the Level 1c and Level 2 SMOS Products with airborne and ground-based observations, in: International Congress on Modelling and Simulation (MODSIM), Perth, Australia, 2011. 9980
Schaefer, G. L., Cosh, M. H., and Jackson, T. J.: The USDA Natural Resources Conservation Service Soil Climate Analysis Network (SCAN), J. Atmos. Ocean. Tech., 24, 2073–2077, 2007. 9963
Scharling, M.: Klimagrid Danmark Nedboer 10 x 10 km (ver.2), Technical Report 99-15, Danish Meteorological Institute, Copenhagen, p. 18, 1999 (in Danish). 9966, 9970
Scheffer, F. and Schachtschabel, P.: Lehrbuch der Bodenkunde, Spektrum Akademischer Verlag GmbH, Heidelberg, Berlin, 2002. 9966
Schou, A.: Atlas over Danmark, 1:750.000, Det Kongelige Danske Geografisk Selskab med

HESSD
8, 9961–10006, 2011

støtte af den Danske Stat, Carlsbergfondet og private virksomheder, H. Hagerup, C. A. Reitzels Forlag, København., 1949. 9970
Smed, P.: Landskabskort over Danmark, 1:360.000, Geografforlaget, 5464 Brenderup, 1979. 9970
Topp, G. C., Davis, J. L., and Annan, A. P.: Electromagnetic determination of soil water content: measurement in coaxial transmission lines, Water Resour. Res., 16, 574–582, 1980. 9966, 9967, 9974, 9975
Vachaud, G., Passerat de Silans, A., Balabanis, P., and Vauclin, M.: Temporal stability of spatially measured soil water probability density function, Soil Sci. Soc. Am. J., 49, 822–828, 1985. 9964
Vasquez, V. and Thomsen, A.: Calibration of a capacitance probe for groundwater recharge modeling based on soil moisture dynamics, in: 1st International Conference and Exploratory Workshop on Soil Architecture and Physio-chemical Functions (CESAR), Faculty of Agricultural Sciences, Aarhus University, Aarhus University Research Center Foulum, Denmark, 2010. 9967
Vejen, F., Madsen, H., and Allerup, P.: Korrektion for fejlkilder påmåling af nedbør – Korrektionsprocenter ved udvalgte stationer 1989–1999, Technical Report 00–20, Danish Meteorological Institute, Copenhagen, p. 53, 2000 (in Danish). 9966
Walker, J. P., Willgoose, G. R., and Kalma, J. D.: The Nerrigundah data set: Soil moisture patterns, soil characteristics, and hydrological flux measurements, Water Resour. Res., 37, 2653–2658, 2001. 9964
Western, A. W. and Bloeschl, G.: On the spatial scaling of soil moisture, J. Hydrol., 217, 203–224, 1999. 9964
Western, A. W., Grayson, R. B., and Bloeschl, G.: Scaling of soil moisture: a hydrologic perspective, Annu. Rev. Earth Pl. Sci., 30, 149–180, 2002. 9963
Wigneron, J.-P., Kerr, Y., Waldteufel, P., Saleh, K., Escorihuela, M.-J., Richaume, P., Ferrazzoli, P., de Rosnay, P., Gurney, R., Calvet, J.-C., Grant, J., Guglielmetti, M., Hornbuckle, B., Mätzler, C., Pellarin, T., and Schwank, M.: L-band Microwave Emission of the Biosphere (L-MEB) Model: Description and calibration against experimental data sets over crop fields, Remote Sens. Environ., 107, 639–655, 2007. 9968

HESSD
8, 9961–10006, 2011

Table 1. Topsoil information (0–20 cm depth): soil type, class numbers used in the sum-up to composite classes, textural fractions [%] of clay (< 2 µm), silt (2–20 µm), fine sand (20–200 µm) and total sand (20–2000 µm), organic matter content (humus 58.7 % C) [%], and respective fractions [%] of soil type contained in the SMOS pixel and working area around node 2 002 029.

Soil type	Recl. val.	Clay	Silt	Fine sand	Total sand	Humus	SMOS pixel	Working area
Coarse sand	10	0–5	0–20	0–50	75–100	<10	79	46
Fine sand	20			50–100			0	3
Coarse loamy sand	30	5–10	0–25	0–40	65–95		13	17
Fine loamy sand	40			40–95			2	13
Coarse sandy loam	50	10–15	0–30	0–40	55–90		0	4
Fine sandy loam	60			40–90			0	9
Clay loam	70	15–25	0–35		40–85		0	2
Humus	90					>10	6	6

HESSD
8, 9961–10006, 2011

Table 2. Subsoil composition (>30 cm depth): soil type, class numbers used in the sum-up to composite classes, clay fractions (<2 µm) [%] and respective fractions [%] contained in the SMOS pixel and working area around node 2 002 029.

Soil type	Recl. val.	Clay	SMOS pixel	Working area
Clay	1	>15	11	30
Sand	2	<10 (mostly < 5)	89	70

HESSD
8, 9961–10006, 2011

Table 3. Land cover information: land cover type, class numbers used in the sum-up to composite classes, and respective fractions [%] contained in the SMOS pixel and working area around node 2 002 029.

Land cover descr		Recl. val.	SMOS pixel	Working area
Artificial surfaces	Urban	100	2	3
	Industry, transport		1	1
	Artificial vegetation		0	1
Agricultural areas	Arable land	200	57	63
	Pastures	300	1	1
	Heterogeneous agriculture	400	16	13
Forest and semi natural areas	Coniferous forests	500	14	11
	Shrub and grassland	600	7	5
Wetlands	Inland wetlands	700	2	1
Water bodies	Inland waters	800	0	1

HESSD
8, 9961–10006, 2011

Table 4. Selected composite classes for the SMOS pixel around node 2 002 029: class number, land cover, top- and subsoil descriptions, respective class fractions [%], corresponding recalculated fractions after redistribution of class 412 and omitting all other classes [%], and numbers of allocated network stations

Class nr.	Land cover	Topsoil	Subsoil	Fract.	Redist. fract.	Nr. stats.
211	Arable land	Coarse sand	Clay	4.3	5.2	2
212	Arable land	Coarse sand	Sand	39.4	55.3	16
232	Arable land	Coarse loamy sand	Sand	5.5	6.7	2
292	Arable land	Humus	Sand	2.9	3.5	2
412	Heterog. agricult.	Coarse sand	Sand	12.1		
512	Forest	Coarse sand	Sand	12.4	15.1	4
612	Heath/shrubs	Coarse sand	Sand	5.6	14.2	4
Others				17.8		

HESSD
8, 9961–10006, 2011

Table 5. Predominant crop types in the Skjern River Catchment, respective estimated fractions [%], number of allocated network stations per crop type and per composite class individually (theoretical and actual distribution).

Crop type	Fractions	Nr. of stations	Nr. stat. 211	Nr. stat. 212	Nr. stat. 232	Nr. stat. 292
Spring barley	28	8	2(1)	2(4)	2(1)	2(1)
Winter barley	7	2	0(0)	2(2)	0(0)	0(0)
Grass	20	5	0(1)	5(3)	0(1)	0(0)
Winter wheat	15	3	0(0)	3(2)	0(0)	0(1)
Maize	5	2	0(0)	2(2)	0(0)	0(0)
Potatoes	4	2	0(0)	2(2)	0(0)	0(0)
Winter rape	4					
Oats	2					
Fallow land	5					
Others	10					

HESSD
8, 9961–10006, 2011

Table 6. Overview of the 30 network stations: station number, latitude, longitude, composite class number, total sand, fine sand, silt, and clay fractions at 0–5 cm depth [%], bulk density (BD) at 0–5 cm depth [g m^{-3}], land cover, and vegetation 2009/2010 and 2010/2011, respectively.

Station Nr.	Lat	Lon	Class Nr.	Sand total	Fine sand	Silt	Clay	BD	Land cover	Vegetation 2009/2010	Vegetation 2010/2011
log1.01	56.02	9.18	612	94.3	18.9	3.5	1.2	1.29	Heath	Grass	Grass
log1.02	56.04	9.16	212	91.7	21.4	5.4	2.3	1.32	Agriculture	Grass/barley	Grass/barley
log1.03	56.03	9.17	612	91.5	11.1	2.4	4.1	1.43	Heath	Scotch heather	Scotch heather
log1.04	56.07	9.33	512	87.3	7.0	4.2	3.0	1.04	Forest	Spruce	Spruce
log1.05	56.03	9.19	512	82.5	15.3	4.4	3.6	1.02	Forest	Spruce	Spruce
log1.06	56.05	9.16	292	90.0	16.1	4.6	2.8	1.20	Agriculture	Spring barley	Potato
log1.07	56.04	9.14	212	90.0	20.3	5.4	3.5	1.31	Agriculture	Grass	Grass
log1.08	56.05	9.12	212	82.2	8.9	5.3	3.3	1.21	Agriculture	Potato	Winter barley
log1.09	56.04	9.13	212	89.5	13.3	4.6	3.2	1.30	Agriculture	Winter barley	Spring barley
log1.10	56.03	9.24	212	93.2	14.6	3.6	2.7	1.19	Agriculture	Maize	Maize
log2.01	55.94	9.22	512	95.8	9.3	1.8	1.3	1.33	Forest	Spruce	Spruce
log2.02	55.98	9.16	212	90.5	8.9	4.0	2.4	1.04	Agriculture	Grass	Grass
log2.03	55.98	9.15	212	86.7	7.9	3.6	1.0	1.28	Agriculture	Potato	Spring barley
log2.04	55.98	9.1	212	87.3	20.9	4.9	7.1	1.21	Agriculture	Potato	Spring barley
log2.05	55.98	9.1	212	87.3	22.6	7.3	4.9	1.22	Agriculture	Spring barley	Potato
log2.06	55.98	9.09	212	93.7	27.7	2.7	3.2	1.41	Agriculture	Grass	Grass
log2.07	55.95	9.03	212	74.9	20.8	7.5	4.6	1.26	Agriculture	Maize	(Winter) Rye
log2.08	55.94	9.03	212	86.3	52.1	7.2	6.4	1.04	Agriculture	Winter wheat	Spring barley
log2.09	55.93	9.12	232	51.1	27.1	28.3	20.6	0.78	Agriculture	Grass	Grass
log2.10	55.99	9.09	612	85.4	5.4	3.5	2.5	1.33	Heath	Scotch heather	Scotch heather
log2.11	55.97	9.02	612	95.7	11.1	2.0	1.7	1.35	Heath	Scotch heather	Scotch heather
log3.01	55.88	9.01	211	79.0	26.2	8.7	5.7	1.30	Agriculture	Spring barley	Potato
log3.02	55.94	8.92	212	90.9	9.4	5.8	3.1	1.31	Agriculture	Spring barley	Spring barley
log3.03	55.91	8.95	212	88.2	23.5	4.3	4.8	1.09	Agriculture	Spring barley	Grass
log3.04	55.91	8.94	212	91.0	39.0	3.2	3.7	1.07	Agriculture	Winter barley	Winter barley
log3.05	55.9	8.92	212	95.0	21.2	3.1	1.6	1.35	Agriculture	Winter wheat	Spring barley
log3.06	55.91	8.88	512	88.9	14.2	5.0	4.8	1.16	Forest	Spruce	Spruce
log3.07	55.91	8.85	292	92.1	15.7	3.8	4.0	0.99	Agriculture	Winter wheat	Spring barley
log3.08	55.88	9.27	211	65.6	36.2	21.0	13.3	1.51	Agriculture	Grass	Grass
log3.09	55.86	9.29	232	85.1	42.9	5.7	5.2	1.26	Agriculture	Spring barley	Grass

HESSD
8, 9961–10006, 2011

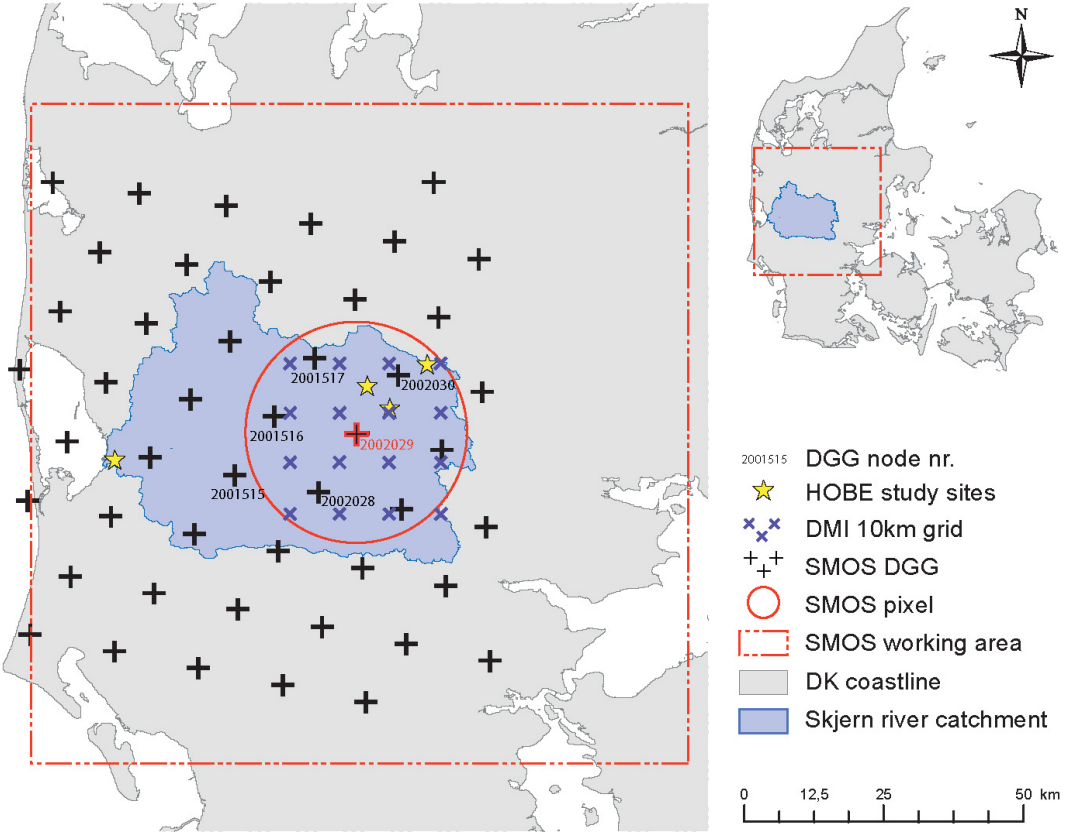

Fig. 1. Skjern Catchment in Western Denmark, HOBE study sites, SMOS Discrete Global Grid (DGG) nodes including numbers of eligible nodes, selected SMOS pixel and corresponding working area around grid node 2 002 029, and DMI 10 km precipitation grid within SMOS pixel.

HESSD
8, 9961–10006, 2011

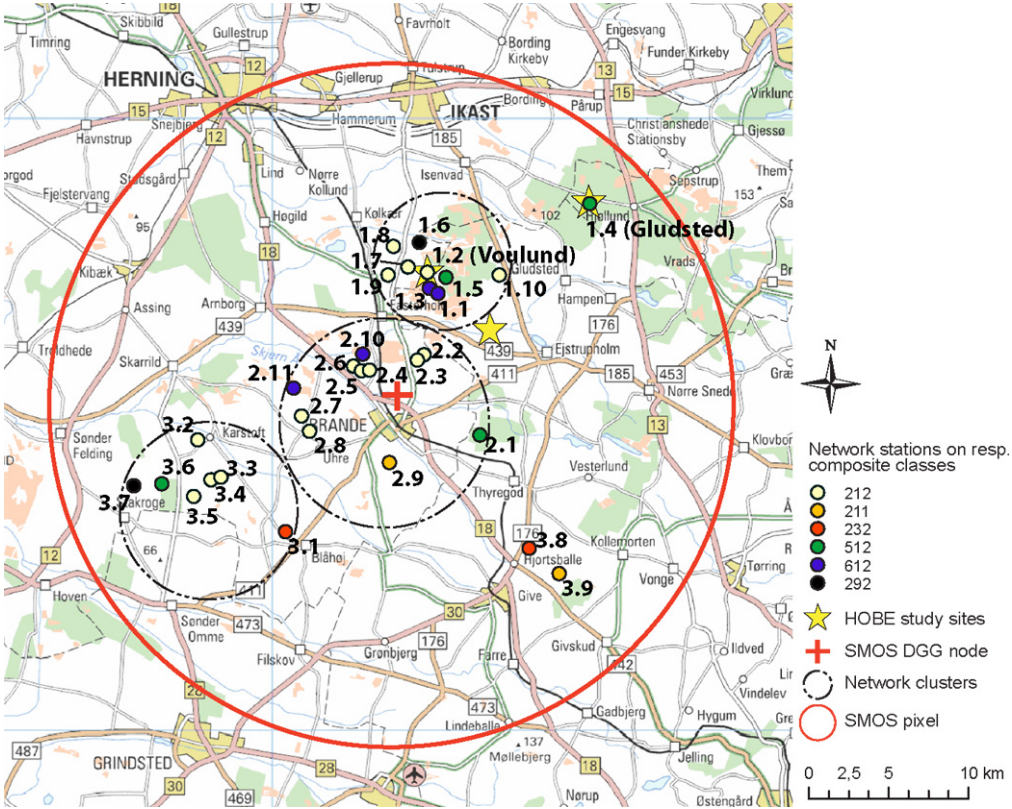

Fig. 2. Overview of the 30 soil moisture network stations installed in the Skjern River Catchment, Western Denmark, within three clusters in the selected SMOS pixel around Discrete Global Grid node 2 002 029.

HESSD
8, 9961–10006, 2011

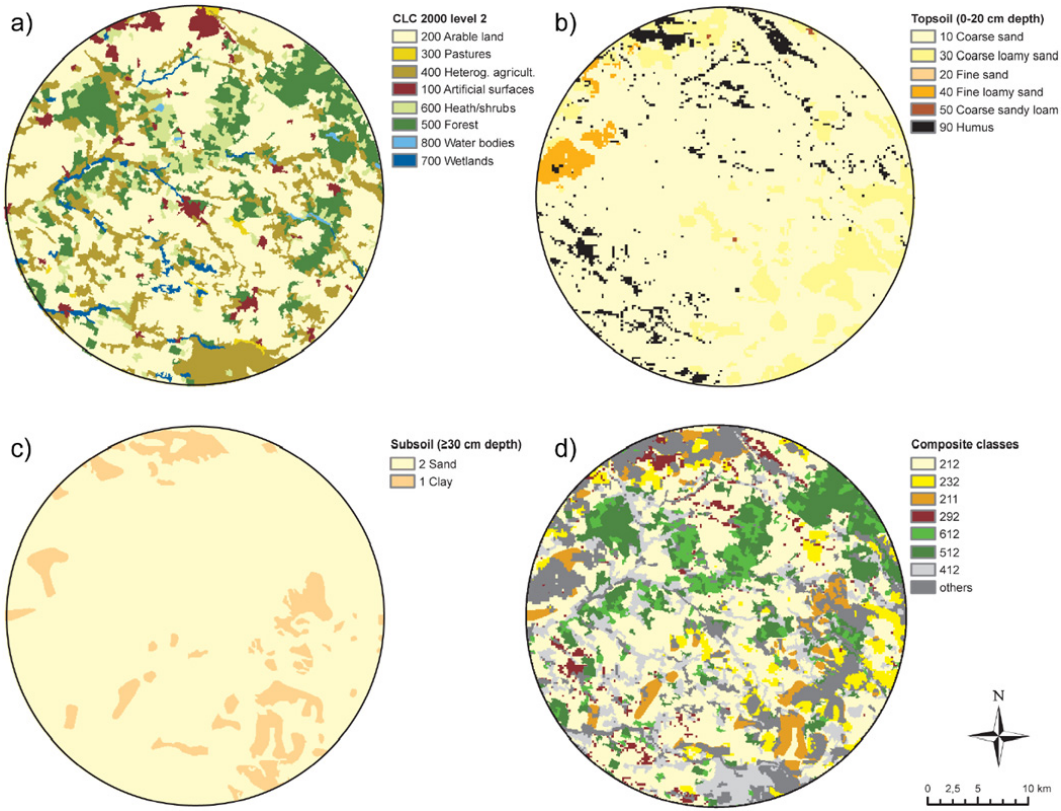

Fig. 3. Land cover type **(a)**, topsoil types **(b)**, subsoil types **(c)** and composite classes, combining land cover type, topsoil and subsoil types **(d)** within the selected SMOS pixel around SMOS Discrete Global Grid node 2 002 029.

HESSD
8, 9961–10006, 2011

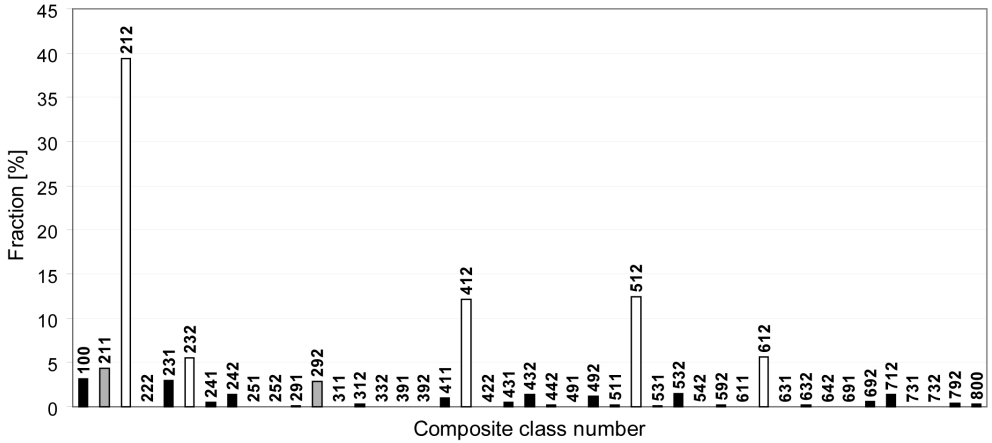

Fig. 4. Fractions [%] of the composite classes (combining land cover, topsoil and subsoil data) contained within the SMOS pixel around node 2 002 029. Classes selected for the placement of network stations with fractions >5 % (212, 232, 412, 512 and 612) are in white, the most frequent classes with humus in topsoil (292)/clay in subsoil (211) are in grey, and the remaining (not considered) classes are in black.

HESSD
8, 9961–10006, 2011

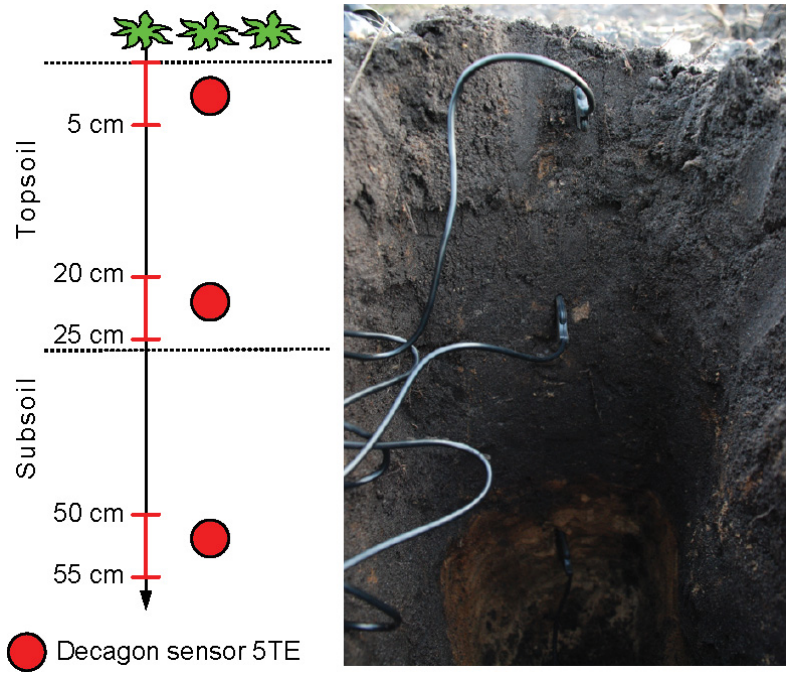

Fig. 5. Schematic sensor configuration at individual network stations (left) using three Decagon 5TE sensors integrating soil moisture over ~5 cm depth intervals, respectively, and photo of soil profile with sensors installed according to the theoretical scheme (right).

HESSD
8, 9961–10006, 2011

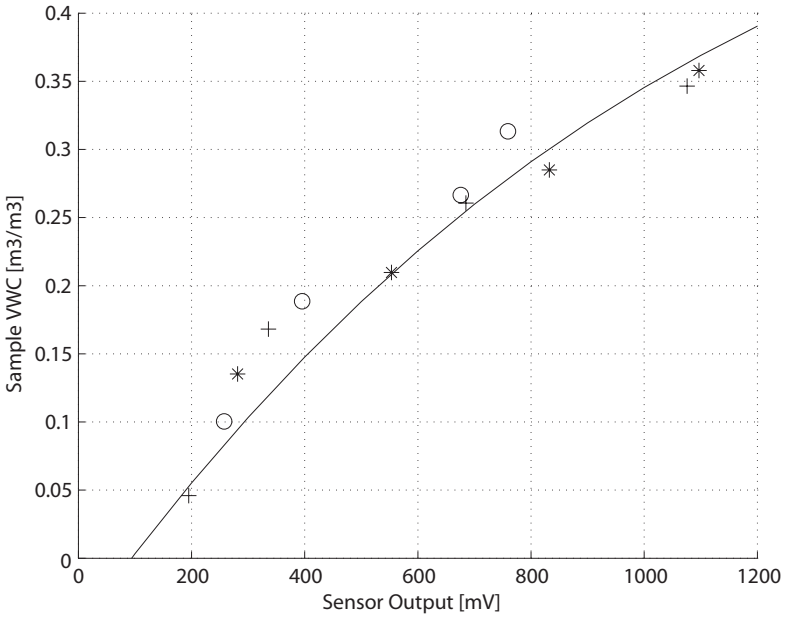

Fig. 6. 5TE sensor output [mV] against volumetric moisture content [$m^3\,m^{-3}$] derived from surface soil samples (0–5 cm depth) of agricultural land (o), forest (+) and heath (∗) (composite classes 212, 512 and 612, respectively) including the Decagon 5TE default calibration curve.

HESSD
8, 9961–10006, 2011

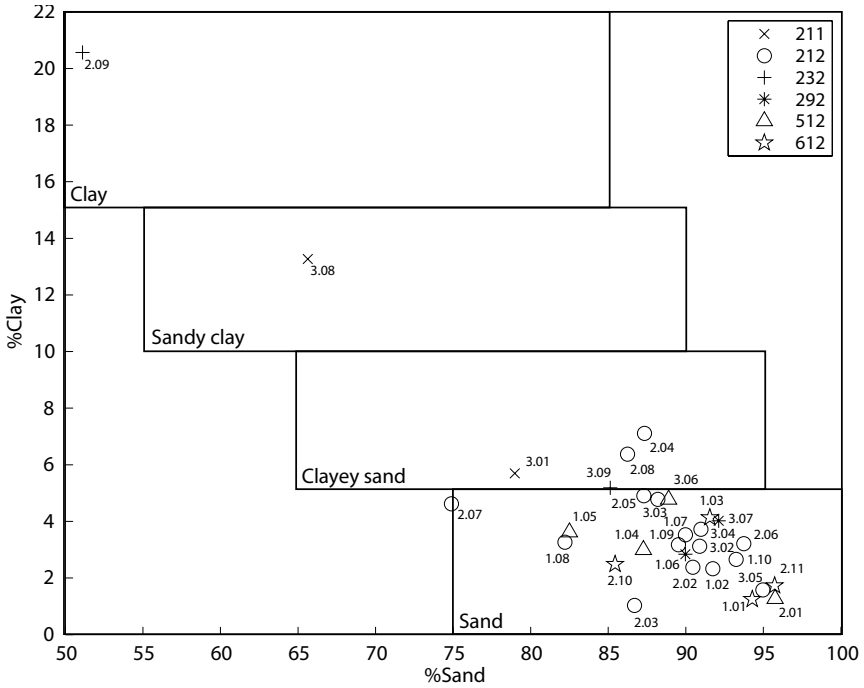

Fig. 7. Soil texture data (sand-% vs. clay-% of 0–5 cm depth) per network station according to the composite classes. Discrimination of zones corresponding to the Danish soil grid (Greve et al., 2007) is also shown.

HESSD
8, 9961–10006, 2011

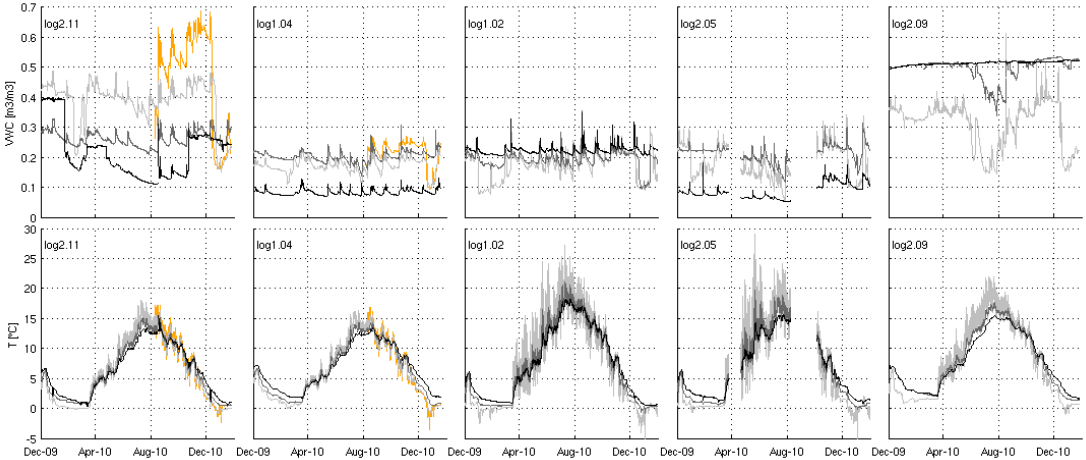

Fig. 8. Profiles of soil moisture (top row) and temperature (bottom row) for the year 2010: for stations 2.11 (heath, class 612), 1.04 (forest, class 512), 1.02 (agriculture, class 212, HOBE site Voulund), 2.05 (agriculture, class 212), and 2.09 (agriculture, class 232); organic layer (orange), mineral soil: 0–5 cm (light grey), 20–25 cm (dark grey), and 50–55 cm (black) depths.

HESSD
8, 9961–10006, 2011

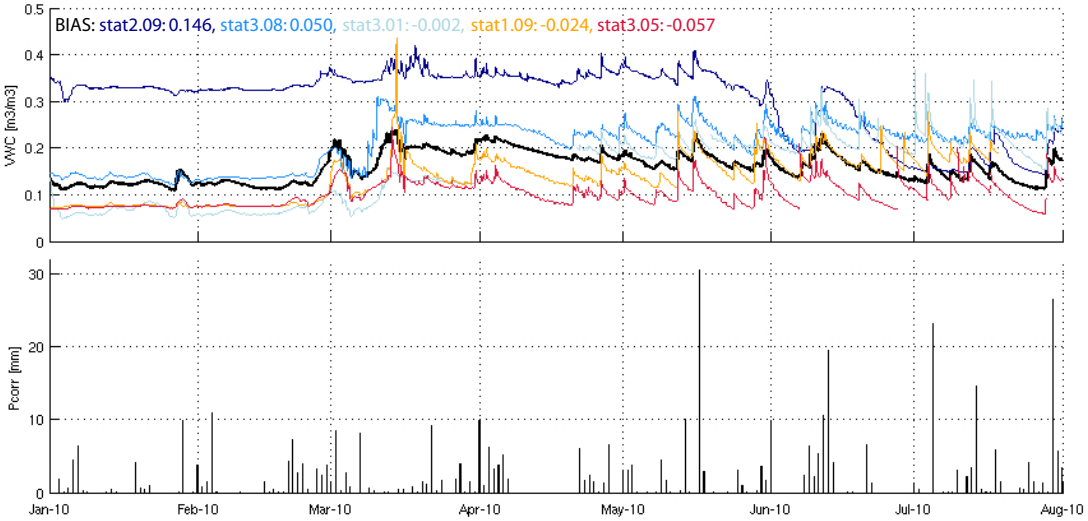

Fig. 9. Surface soil moisture (0–5 cm) with decreasing/increasing clay/sand fractions, respectively, between January and August 2010: agricultural stations 2.09 (dark blue), 3.08 (blue), 3.01 (light blue), 1.09 (orange) and 3.05 (red) compared to the average of all 30 network stations (black) (top row) including corresponding biases; and mean of daily precipitation of the DMI 10 km grid nodes contained within the SMOS pixel (bottom row).

HESSD
8, 9961–10006, 2011

Fig. 10. Regional surface soil moisture and temperature (0–5 cm) for the year 2010: Average and standard deviation (shaded regions) of the 0–5 cm soil moisture (top row) and temperature (center row) of three selected stations of similar texture and land cover in the north-east (1.02, 106, 1.09, red) and south-west part (3.02, 3.04, 3.07, black) of SMOS pixel 2 002 029 as well as daily precipitation of the two closest 10 km grid nodes, resp., (bottom row) including corresponding RMSE, bias and R^2 values. During periods where the shaded regions are absent, only one sensor was operational per area.

HESSD
8, 9961–10006, 2011

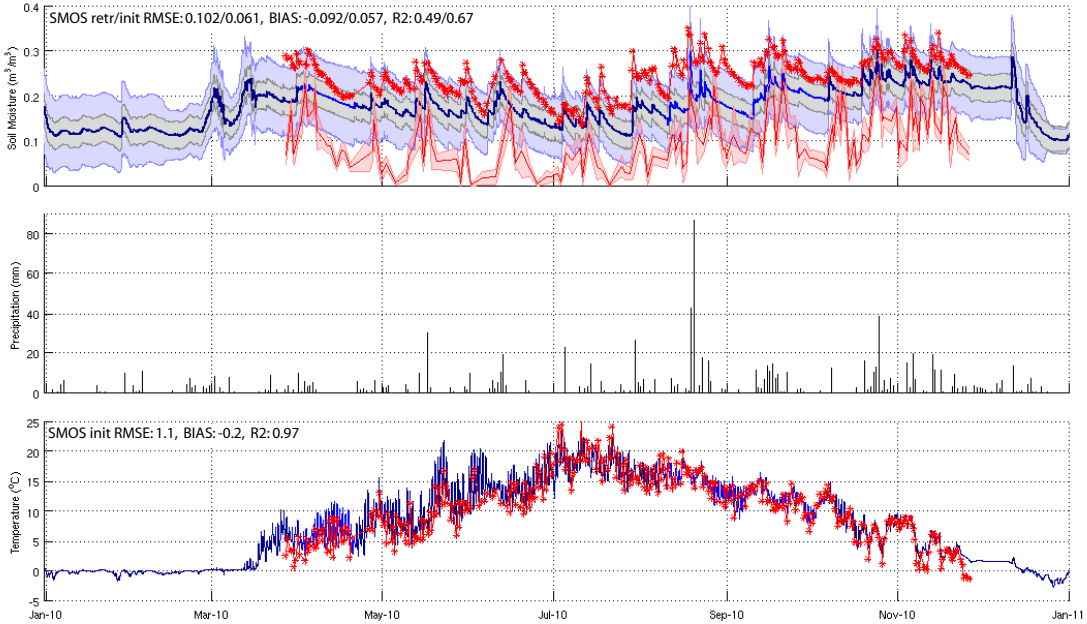

Fig. 11. Surface soil moisture and temperature (0–5 cm) comparison between network and SMOS for the year 2010: surface soil moisture network average and standard deviation (blue lines* and shaded region) including sensor accuracy (grey-shaded region), and retrieved SMOS soil moisture (red line) including radiometric accuracy (red-shaded region) and corresponding initial guess (red stars, top row); mean of daily precipitation of the DMI 10 km grid nodes contained within the SMOS pixel (center row); temperature network average (blue lines*) and SMOS initial guess (red stars, bottom row). RMSE, bias and R^2 of the in situ versus retrieved/initial SMOS data for soil moisture and temperature are indicated. *dark blue where >20, royal blue where <20 stations operational.

HESSD
8, 9961–10006, 2011